Journal of Power Sources 295 (2015) 74–78

Contents lists available at ScienceDirect

Journal of Power Sources

journal homepage: www.elsevier.com/locate/jpowsour

Effects of surface chemistry and microstructure of electrolyte on oxygen reduction kinetics of solid oxide fuel cells

Joong Sun Park [a, b], Jihwan An [b, c], Min Hwan Lee [d], Fritz B. Prinz [b, e], Wonyoung Lee [b, f, *]

[a] Chemical Sciences and Engineering Division, Argonne National Laboratory, USA
[b] Department of Mechanical Engineering, Stanford University, USA
[c] Manufacturing Systems and Design Engineering Program, Seoul National University of Science and Technology, Republic of Korea
[d] Department of Mechanical Engineering, University of California, Merced, USA
[e] Department of Materials and Science Engineering, Stanford University, USA
[f] School of Mechanical Engineering, Sungkyunkwan University, Republic of Korea

HIGHLIGHTS

- Enhanced surface kinetics with increase in grain boundary density.
- Mobile oxygen vacancies populated at grain boundaries.
- Oxygen vacancies induced by Y^{3+} surface segregation were found to be inactive.
- Our results provide guidelines to engineer the electrolyte–electrode interfaces.

GRAPHICAL ABSTRACT

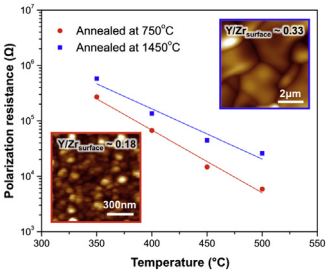

ARTICLE INFO

Article history:
Received 13 December 2014
Received in revised form
9 June 2015
Accepted 29 June 2015
Available online 10 July 2015

Keywords:
Solid oxide fuel cells
Cathode
Oxygen reduction kinetics
Grain boundary

ABSTRACT

We report systematic investigation of the surface properties of yttria-stabilized zirconia (YSZ) electrolytes with the control of the grain boundary (GB) density at the surface, and its effects on electrochemical activities. The GB density of thin surface layers deposited on single crystal YSZ substrates is controlled by changing the annealing temperature (750–1450 °C). Higher oxygen reduction reactions (ORR) kinetics is observed in samples annealed at lower temperatures. The higher ORR activity is ascribed to the higher GB density at the YSZ surface where 'mobile' oxide ion vacancies are more populated. Meanwhile, oxide ion vacancies concurrently created with yttrium segregation at the surface at the higher annealing temperature are considered inactive to oxygen incorporation reactions. Our results provide additional insight into the interplay between the surface chemistry, microstructures, and electrochemical activity. They potentially provide important guidelines for engineering the electrolyte–electrode interfaces of solid oxide fuel cells for higher electrochemical performance.

1. Introduction

Fluorite-structured oxides, such as yttria-stabilized zirconia (YSZ) and gadolinia-doped ceria (GDC), are widely used as solid-state electrolytes for electrochemical energy conversion devices. Among them, YSZ is one of the most commonly used electrolyte materials, due to its chemical stability with reasonably high ionic conductivity for solid oxide fuel cells (SOFCs) [1–3]. In this material, interfacial properties often dominate the electrochemical performances at low temperature operation. First, the properties of surface, the interface between the material and the atmosphere, are often the determining factor for the overall device performance,

* Corresponding author. School of Mechanical Engineering, Sungkyunkwan University, Suwon 440-746, Republic of Korea.
E-mail address: leewy@skku.edu (W. Lee).

http://dx.doi.org/10.1016/j.jpowsour.2015.06.149
0378-7753/

especially in the thin film devices. For example, Chao et al. showed that the 1 nm thick YSZ surface modification layer, in which the concentration of oxide ion vacancies was controlled to be higher than that of bulk YSZ, significantly enhanced the surface exchange coefficient [4]. Second, the grain boundary (GB; i.e. inter-granular interface) plays a crucial role in the ionic transport and exchange reactions. Ionic transport across GBs is known to be hindered due to an electrical potential barrier built up by defect segregation [5,6], while exchange reaction is enhanced near the GBs, due to the higher concentration of oxide ion vacancies [7–11].

Several studies have been reported on the systematic control of GB density near the surface by thermal annealing processes to enhance the surface exchange rate and electrochemical performance in various fluorite-based materials [8–11]. The surface exchange rate increased with the GB density at the surface. However, thermal annealing may affect not only the GB density, but also the chemical composition due to segregation of defects and ions [12–14]. Dopant segregation at the surface is important in cathode reactions in SOFCs since it can affect the near-surface chemical reactions and ionic transport of the electrolytes [15–18]. The correlation between the observed surface exchange rate and the surface defect segregation level has not yet been elucidated, even though those two factors are highly likely to be correlated each other.

In this study, we present a systematic investigation of the YSZ surface properties with the control of GB density at the surface, and its effects on electrochemical activities. The GB density in the thin surface layers deposited on polycrystalline YSZ substrates was controlled by the temperature of annealing process (750–1450 °C). With the higher annealing temperature, the grain size became larger resulting in a lower GB density, and the oxide ion vacancies at the surface became more populated by enhanced dopant segregation. The reduction of GB density at the surface may decrease the oxygen reduction reaction (ORR) rates while a higher concentration of oxide ion vacancies may increase the reaction sites for ORR. We present a comprehensive discussion through various characterizations on the material and electrochemical properties with the aid of atomic force microscopy (AFM), X-ray diffraction (XRD), angle-resolved X-ray photoemission spectroscopy (AR-XPS), and electrochemical impedance spectroscopy (EIS). Such a systematic quantification of the temperature-induced changes in the electrolyte surfaces provides enhanced understanding on the interplay between the surface chemistry, microstructures, and electrochemical activity, which may lead to the capability to further engineer functional materials for higher performance.

2. Experimental

Thin film YSZ with a thickness of ~500 nm was deposited on 500 μm thick polycrystalline YSZ substrates (Ceraflex 8YSZ) by pulsed laser deposition (PLD), using a Lambda Physik 248 nm KrF excimer laser with a fluence of 1.5 J/cm^2 per pulse. The substrate temperature was kept at 750 °C during deposition. The oxygen pressure was 100 mTorr and 200 Torr for deposition and cooling, respectively. The samples were annealed in air at a temperature between 750 and 1450 °C for 10 h to control the surface microstructures. Porous Pt with a thickness of ~80 nm was deposited on both sides of the samples by DC sputtering at an Ar pressure of 10 Pa.

A commercial AFM system (JSPM5200, JEOL) was used to characterize the surface morphology in the tapping mode. XRD patterns were obtained with Bruker D2 phaser instrument (Cu K_α with $\lambda = 1.5406$ Å) with a scan rate of 1°/min and 0.05° step size. AR-XPS was used to identify the cation chemistries of YSZ film surfaces. Phi Versa Probe XPS microscope was operated with Al K_α X-ray (1486 eV) at 200 W for spectral analysis and compositional quantification. Spectra were acquired with emission angles from 15° to 75°, as defined relative to the surface normal. For the excitation energy of 1486 eV, the sampling depths of these photoelectrons at the emission angle of 15° are ~6.8 nm for both Zr 3d and Y 3d, considering the inelastic mean free path of photoelectrons. At the emission angle of 75°, on the other hand, the sampling depths of both elements are ~1.8 nm, making the measurements significantly more surface sensitive [17,19]. Spectra were acquired twice, to reveal the distribution of chemical composition in the thickness direction. This was done by subsequent acquisition; first, from the as-annealed surfaces; and second, after Ar etching to remove the surface layer of approximately 2–3 nm. Y $3d_{3/2}/3d_{5/2}$ and Zr $3d_{3/2}/3d_{5/2}$ peaks were used for the peak integration. Conditions for Ar etching in XPS were 5 kV, 1 uA and 2 × 2 mm^2 of area. Etching rate of the films was back calculated by depth profiling. EIS measurements were performed using a Gamry FAS2 Femtostat system at 350, 400, 450, and 500 °C in the frequency range of 300 kHz–0.1 Hz with an AC signal amplitude of 50 mV. Hydrogen was fed at the anode with 10 sccm while the cathode was exposed to atmospheric air. The EIS results were analyzed and fitted to the spectra based on a complex nonlinear least squares fitting method. Details of sample setups including gas feedings and substrate heating, was previously described [20–22].

3. Results and discussion

First, we performed a structural analysis with AFM and XRD, to explore the effects of thermal annealing on the surface microstructures. The change of thermal annealing temperature was intended to control the GB density in the surface layers. Fig. 1 shows the surface morphology of YSZ samples annealed at different temperatures. The grain sizes varied from ~50 nm to ~5 μm, depending on the annealing temperature from 750 °C to 1450 °C. Assuming a constant GB width regardless of annealing temperature, the GB density decreased by a factor of 20–100, with the increase of the annealing temperature from 750 °C to 1450 °C. As was found in our earlier observations, the grain growth induced by thermal annealing enabled us to control the GB density at the surface [8–11]. Fig. 2 shows X-ray diffraction patterns from the YSZ samples annealed at 750 °C and 1450 °C. The patterns showed no noticeable difference between samples, indicating that no significant secondary phases or impurities were evolved during the thermal annealing within a resolution of XRD used here. These results substantiate that the thermal annealing enabled the control of the GB density in the surface layers without generating undesired phases.

To find the correlation between the GB density near the YSZ surface and electrochemical activity, we performed a series of EIS measurements at 350–500 °C. Fig. 3 shows representative Nyquist plots measured at 500 °C from the YSZ samples annealed at 750 °C and 1450 °C under $V_{DC} = 0.5$ V with respect to the reference electrode connected to the anode. The anode and cathode were exposed to pure dry hydrogen and ambient air, respectively. The impedance spectra with porous Pt electrodes showed two distinct arcs. The arc at the high frequencies is known to describe charge transport through the electrolyte, associated with oxide ion diffusion through the grains and the grain boundaries in the bulk electrolyte [23–25]. The magnitude of arc at the high frequencies showed no appreciable distinction between samples and the calculated oxide ion conductivities matched well with reported values (see Fig. S1) [2,21,22,26]. Although the oxide ion diffusivity across GBs is known to be several orders lower than that through grains [5,27–29], the obtained high frequency arc shows no discernible difference between the samples. (Note that two

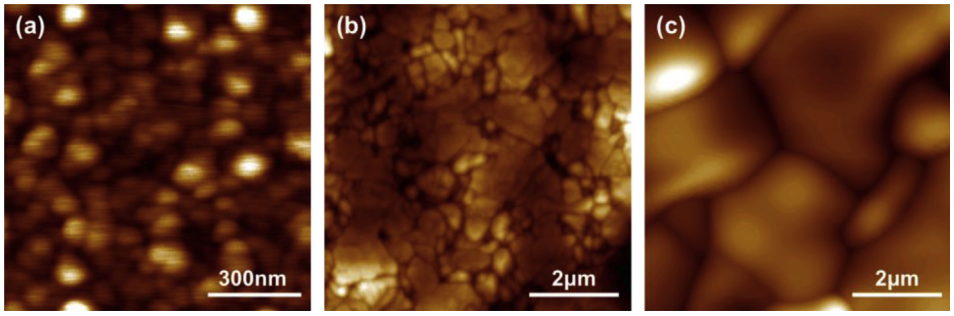

Fig. 1. AFM images of the YSZ surfaces annealed at (a) 750 °C, (b) 1100 °C, and (c) 1450 °C.

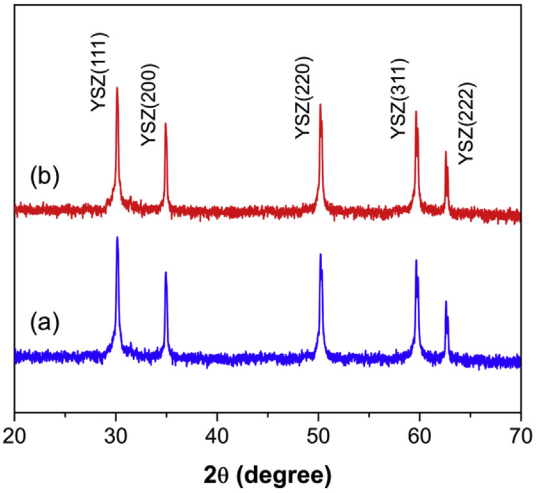

Fig. 2. XRD patterns of the YSZ samples annealed at (a) 750 °C and (b) 1450 °C.

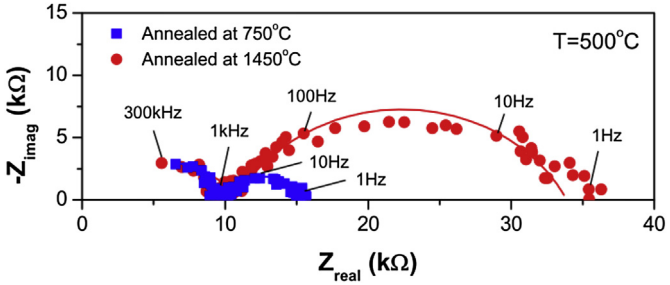

Fig. 3. Electrochemical impedance spectra of YSZ samples annealed at 750 °C (blue) and 1450 °C (red) with the DC bias (V_{DC}) of 0.5 V. Measurements were done at 500 °C with H_2 fed at anode side and air at cathode side. (For interpretation of the references to color in this figure legend, the reader is referred to the web version of this article.)

samples had different GB densities near the YSZ surface by a factor of 20–100.) This result can be ascribed to the fact that the surface layer was ~500 nm thick, and contributed only a fraction of 10^{-3} to the overall Ohmic resistance. Moreover, films deposited by PLD are known to form columnar structures [30,31], in which there is little GBs to diffuse across. On the other hand, the low frequency arc is known to originate from charge transfer reactions at the electrode/electrolyte interfaces, and its size is negatively correlated to ORR activity [23–25]. The magnitude of arc at the low frequencies showed a positive correlation with the annealing temperature; the higher annealing temperature of YSZ, the larger the low frequency arc of the corresponding cell. It is generally known that the cathodic impedance dominates the total impedance of the electrode, while the anodic impedance is negligible, especially in the temperature range probed in this study [9,20,25,32,33]. Therefore, the observed correlation between the low frequency impedance and the annealing temperature effectively reveals that the cathodic impedance increases with the annealing temperature, which can be attributed to the decreased GB density at the surface. In general, oxide ions incorporate into the electrolyte through oxide ion vacancies at the surface. Recent experimental and theoretical studies have been reported that oxide ion vacancies were populated near the grain boundaries in fluorite-structured oxide materials [8–13]. Hence, a lower GB density should result in a decrease in the concentration of the oxide ion vacancies (i.e. reaction sites) at the surfaces required for oxygen incorporation. Therefore, higher annealing temperature reduced the GB density (the density of reaction sites for oxygen incorporation), which in turn increased the electrode polarization impedance.

The observed correlation between the ORR kinetics and the GB density substantiated the non-uniform distribution of the oxide ion vacancies or the reaction sites for oxygen incorporation. However, whether the GB density was the only change made by the thermal annealing remains as an open question. The thermal annealing may induce changes in surface chemistry, which significantly impact ORR kinetics at the electrolyte surface [4,12]. To address how surface chemistry can change upon the thermal annealing at different temperatures, we designed experiments using AR-XPS to probe the chemical composition of the surface and the bulk in a non-destructive way [17,18]. Two incidence angles of 15° and 75° (defined from the surface normal) were selected with an approximate information depth of 6.8 nm and 1.8 nm from the top surface, respectively (see Fig. S3).

Fig. 4 shows the Y/Zr concentration ratio at the two different incident angles as a function of annealing temperature. After an annealing at 750 °C, Y/Zr ratios were similar at both incident angles, and the calculated molar concentrations of yttria were close to 8 mol% as expected. At higher annealing temperature, however, the Y/Zr ratio between the two incident angles diverged. Higher Y/Zr ratios were observed at the incident angle of 75°, indicating the higher concentration of yttrium toward the surface. Further, the degree of yttrium segregation became more pronounced with annealing temperatures; the effective molar concentrations of yttria at the surface were 11 and 14 mol% at 1100 °C and 1450 °C, respectively. The degree of yttrium segregation at the surface was consistent with other experimental and theoretical observations, which showed Y/Zr ratios of 0.3–0.37 with XPS, ~0.44 with low-energy ion scattering (LEIS), and ~0.35 with molecular dynamics (MD) simulations [12,14,34,35]. When the top surface (~2 nm) was etched by Ar ion, Y/Zr values at the incident angle of 75° decreased and became similar to those at the incident angle of 15°. Y/Zr values at the incident angle of 15°, however, remained unchanged after Ar ion etching. The different sampling depth with two incident angles

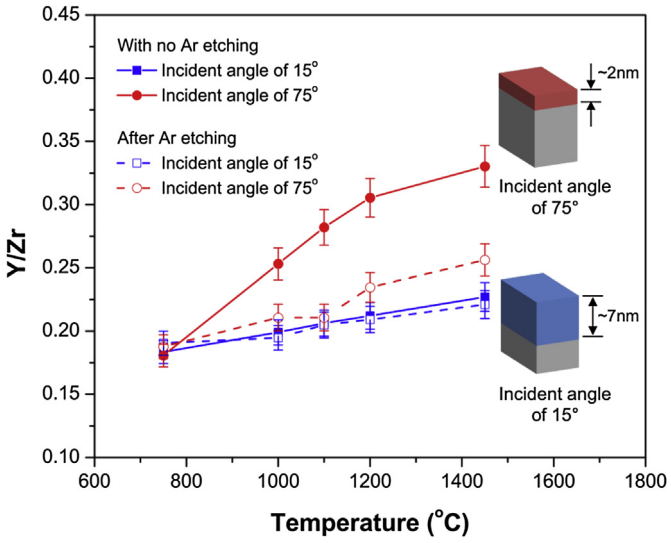

Fig. 4. Y/Zr concentration ratio as a function of the annealing temperature.

suggests that the observed yttrium segregation occurred mostly at the topmost surface of approximately 2 nm. Previous observations by LEIS experiments and MD simulations showed that the dopant segregation mostly occurred within a few atomic layers from the topmost surface, which agrees well with our AR-XPS observation [12,35]. In our case, even after the Ar ion etching, Y/Zr ratios measured at the incident angle of 75° were still higher than those at 15°. This can be interpreted as the yttrium segregation being more promoted with higher annealing temperature, resulting in a relatively thicker layer with the yttrium segregation.

We believe that the higher Y/Zr ratio, and thus the higher molar concentration of yttria, was closely associated with the higher concentration of oxide ion vacancies at the surfaces [12]. Thermal annealing above 750 °C may create excess oxide ion vacancies at the surface given that oxide ion vacancies are generated via the introduction of trivalent yttrium [36]; the localized concentration of oxide ion vacancies at the surface is expected to be high, concurrently with the surface segregation of yttrium. Such surface segregation of yttrium may enhance the oxygen incorporation kinetics, as recently reported by Chao et al. [4,37] They demonstrated that an intentional high-doping of yttrium (14 mol%) at the surface rendered a significant enhancement of the oxygen incorporation kinetics, and of the resulting fuel cell performance.

From the discussions above, oxide ion vacancies at and near the surface can be more populated with i) higher GB density, and ii) more dopant segregation. For a maximized performance, the annealing temperature needs to be optimized because higher annealing temperature promotes dopant segregation by compromising the GB density. A simple calculation was attempted to answer which of the two factors has higher impact on the oxygen reduction activity. The concentration of oxide ion vacancy (per area) can be expressed by the sum of vacancy concentrations in the grain and at the grain boundary. Since the length scale of grains (50 nm–5 μm) is far greater than that of grain boundaries (1–2 nm) [5,7,38], the overall concentration of oxide ion vacancy is expected to be more influenced by the dopant segregation at the surface than the GB density itself, unless the sizes of grains and grain boundaries are comparable.

The relative impact of dopant segregation and grain boundary density on electrode impedance was studied by an EIS analysis. Fig. 5 shows the electrode impedances as a function of the annealing temperatures, which correspond to the size of the lower frequency arcs in the Nyquist plot (see Fig. S2). The Nyquist plots were analyzed with Z-plot software based on complex nonlinear least-square fitting with two parallel resistance-constant phase element. Activation energies of polarization resistances were extracted from Arrhenius relation. Calculated activation energy, E_a, for samples annealed at 750 °C (with the high GB density) and 1450 °C (with the low GB density) were 0.87 ± 0.02 eV and 1.08 ± 0.03 eV, respectively. The low activation energy for interfacial impedance (i.e. oxygen reduction reaction at samples with the high GB density at surface) suggests that incorporation at grain boundaries is energetically more favorable than that of bulk. Our previous work also showed the preferential oxygen incorporation at grain boundaries with DFT simulations [43]. The YSZ sample annealed at 750 °C, having the highest GB density and the least dopant segregation, exhibited the smallest electrode impedance. In other words, oxide ion vacancies induced by dopant segregation at the surface did not play a dominant role in the improvement of ORR kinetics. We speculate that oxide ion vacancies created by dopant segregation may not actively participate in oxygen incorporation, due to vacancy (positively charged) – dopant (negatively charged) interactions, where the migration barrier of oxygen to hop Y–Zr or Y–Y is much higher than that of Zr–Zr [39]. In addition, vacancy–vacancy pairs moves more slowly than a single vacancy, explaining low oxide ion diffusivity in a highly doped zirconia [40]. These defect-associated interactions may ultimately reduce the concentration of mobile oxide ion vacancies at the surface, even with the higher concentration of total oxide ion vacancies. Oxide ion vacancies populated at grain boundaries, however, were relatively easier to move because of the relaxed structures, which may facilitate incorporation reactions [13]. We can also speculate on the possibility of generating a higher incorporation barrier at the yttrium-rich surface during the thermal annealing at the high temperature. It has been reported that the outmost layer of YSZ can be covered with the yttrium-rich layer and monoclinic YSZ subsurface layers. The oxide ion diffusivity in these surface layers was found to be several orders of lower than that of bulk YSZ [35,41]. In sum, the annealing-induced segregation of yttrium at the surface may not improve the ORR kinetics due to the defect-associated interactions and the higher incorporation barrier. Furthermore, the GB density at the surface, where the concentration of oxide ion vacancies is higher than grain, plays a significant

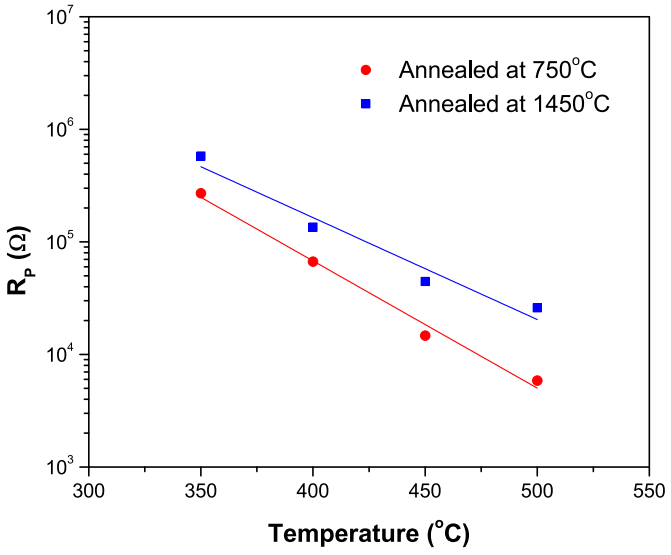

Fig. 5. Arrhenius plot of electrode polarization resistance of YSZ samples annealed at 750 °C and 1450 °C.

role in the improvement of the ORR kinetics.

We also compared the surface roughness and the surface area of the YSZ samples. A higher surface roughness can provide additional sites for surface reactions and thus reduces the cathodic impedance. An AFM topography scan in an area of 10 × 10 μm^2 revealed that the RMS roughness were 15 and 34 nm, and the actual surface areas were 101.8 and 100.3 μm^2 for the samples annealed at 750 °C and 1450 °C, respectively. There were no significant difference between the two samples in terms of the surface roughness and surface area. Depth profiling with XPS confirmed that the chemical composition of the YSZ substrates remained unchanged after thermal annealing. AFM and scanning electron microscopy (SEM) were employed to examine the microstructure of the Pt electrode, which can be affected by the underlying YSZ films [42]. The grain size of the Pt electrode was 30–50 nm for both samples, and there was no appreciable difference in the surface morphology in a larger area, as the samples showed similar porous structures. After EIS measurements, the microstructural coarsening occurred in both samples due to Ostwald ripening. However, the microstructures of the Pt electrode remained still porous, showing no noticeable differences between samples [43]. These results substantiate that the observed enhancement in the surface reactivity originates not from the changes in the surface morphology or the chemical composition of the additional electrolyte layer and electrode, but from the difference in the surface microstructures, represented by the GB density. Lastly, XPS scans for impurities were performed on the annealed surfaces. Impurities including silicon, alkali metals, and transition metals might be segregated near grain boundaries or form the layer at the surface to deteriorate the oxygen reduction kinetics. However, no impurities were found within a resolution of XPS used in this study, we excluded effects of impurities on oxygen reduction kinetics at annealed samples at elevated temperatures.

4. Conclusions

In summary, we have investigated the effects of surface chemistry and microstructure on ORR kinetics, by controlling the degree of dopant segregation and grain size of YSZ, especially at the surface region. Thermal annealing resulted in a grain growth decreasing the effective GB density, and simultaneously induced yttrium segregation to the electrolyte surface. A higher GB density and more dopant segregation would increase the concentration of oxide ion vacancies at the surface, and thus enhance ORR activities. In this study, we confirm that increasing the GB density by lowering the annealing temperature is more effective in enhancing the oxygen incorporation kinetics, rather than boosting the yttrium segregation by increasing the annealing temperature. These results suggest that oxide ion vacancies populated at grain boundaries participated more actively in oxygen incorporation reactions while those created by dopant segregation were likely to be bound to neighboring defects, and thus inactive to oxygen incorporation reactions.

Acknowledgments

This research was supported by Basic Science Research Program through the National Research Foundation of Korea (NRF) funded by the Ministry of Science, ICT & Future Planning (Grant No. NRF-2013R1A1A1059845), and by the Global Frontier R&D Program on Center for Multiscale Energy System funded by the National Research Foundation under the Ministry of Science, ICT & Future Planning, Korea (Grant No. NRF-2014M3A6A7074784).

Appendix A. Supplementary data

Supplementary data related to this article can be found at http://dx.doi.org/10.1016/j.jpowsour.2015.06.149.

References

[1] S.B. Adler, Chem. Rev. 104 (2004) 4791.
[2] B.C.H. Steele, A. Heinzel, Nature 414 (2001) 345.
[3] J. An, J.H. Shim, Y.B. Kim, J.S. Park, W. Lee, T.M. Gur, F.B. Prinz, MRS Bull. 39 (2014) 798.
[4] C.-C. Chao, Y.B. Kim, F.B. Prinz, Nano Lett. 9 (2009) 3626.
[5] X. Guo, J. Maier, J. Electrochem. Soc. 148 (2001) E121.
[6] J.S. Park, Y.-B. Kim, J. An, F.B. Prinz, Solid State Commun. 152 (2012) 2169.
[7] J. An, J.S. Park, A.L. Koh, H.B. Lee, H.J. Jung, J. Schoonman, R. Sinclair, T.M. Gür, F.B. Prinz, Sci. Rep. 3 (2013).
[8] Y.B. Kim, J.S. Park, T.M. Gür, F.B. Prinz, J. Power Sources 196 (2011) 10550.
[9] W. Lee, H.J. Jung, M.H. Lee, Y.B. Kim, J.S. Park, R. Sinclair, F.B. Prinz, Adv. Funct. Mater. 22 (2012) 965.
[10] J.H. Shim, J.S. Park, T.P. Holme, K. Crabb, W. Lee, Y.B. Kim, X. Tian, T.M. Gür, F.B. Prinz, Acta Mater. 60 (2012) 1.
[11] J.H. Shim, S. Kang, S.W. Cha, W. Lee, Y.B. Kim, J.S. Park, T.M. Gur, F.B. Prinz, C.C. Chao, J. An, J. Mater. Chem. A 1 (2013) 12695.
[12] H.B. Lee, F.B. Prinz, W. Cai, Acta Mater. 58 (2010) 2197.
[13] H.B. Lee, F.B. Prinz, W. Cai, Acta Mater. 61 (2013) 3872.
[14] A. Hughes, B. Sexton, J. Mater. Sci. 24 (1989) 1057.
[15] M. De Ridder, A.G.J. Vervoort, R.G. van Welzenis, H.H. Brongersma, Solid State Ion. 156 (2003) 255.
[16] K.C. Lau, C.H. Turner, B.I. Dunlap, Chem. Phys. Lett. 471 (2009) 326.
[17] W. Lee, J.W. Han, Y. Chen, Z. Cai, B. Yildiz, J. Am. Chem. Soc. 135 (2013) 7909.
[18] Z. Cai, M. Kubicek, J. r. Fleig, B. Yildiz, Chem. Mater. 24 (2012) 1116.
[19] Nist Database 82, U.S. Department of Commerce, 2001.
[20] H. Huang, M. Nakamura, P. Su, R. Fasching, Y. Saito, F.B. Prinz, J. Electrochem. Soc. 154 (2007) B20.
[21] J.H. Shim, C.-C. Chao, H. Huang, F.B. Prinz, Chem. Mater. 19 (2007) 3850.
[22] P.-C. Su, C.-C. Chao, J.H. Shim, R. Fasching, F.B. Prinz, Nano Lett. 8 (2008) 2289.
[23] H.J. Avila-Paredes, K. Choi, C.-T. Chen, S. Kim, J. Mater. Chem. 19 (2009) 4837.
[24] E. Barsoukov, J.R. Macdonald, Impedance Spectroscopy: Theory, Experiment, and Applications, John Wiley & Sons, 2005.
[25] H.L. Tuller, S.J. Litzelman, W. Jung, Phys. Chem. Chem. Phys. 11 (2009) 3023.
[26] B.C.H. Steele, Solid State Ion. 75 (1995) 157.
[27] C. Leach, P. Tanev, B. Steele, J. Mater. Sci. Lett. 5 (1986) 893.
[28] M. Aoki, Y.M. Chiang, I. Kosacki, L. Lee, H. Tuller, Y. Liu, J. Am. Ceram. Soc. 79 (1996) 1169.
[29] C. Peters, A. Weber, B. Butz, D. Gerthsen, E. Ivers-Tiffée, J. Am. Ceram. Soc. 92 (2009) 2017.
[30] Y.B. Kim, T.M. Gür, S. Kang, H.-J. Jung, R. Sinclair, F.B. Prinz, Electrochem. Commun. 13 (2011) 403.
[31] W. Jung, J.O. Dereux, W.C. Chueh, Y. Hao, S.M. Haile, Energ. Environ. Sci. 5 (2012) 8682.
[32] S. De Souza, S.J. Visco, L.C. De Jonghe, Solid State Ion. 98 (1997) 57.
[33] T.P. Holme, R. Pornprasertsuk, F.B. Prinz, J. Electrochem. Soc. 157 (2010) B64.
[34] A. Bernasik, K. Kowalski, A. Sadowski, J. Phys. Chem. Solids 63 (2002) 233.
[35] M. De Ridder, R. Van Welzenis, A.D. Van der Gon, H. Brongersma, S. Wulff, W.-F. Chu, W. Weppner, J. Appl. Phys. 92 (2002) 3056.
[36] R.P. O'Hayre, S.-W. Cha, W. Colella, F.B. Prinz, Fuel Cell Fundamentals, John Wiley & Sons, 2006.
[37] C.-C. Chao, J.S. Park, X. Tian, J.H. Shim, T.M. Gür, F.B. Prinz, ACS Nano 7 (2013) 2186.
[38] J. An, A.L. Koh, J.S. Park, R. Sinclair, T.M. Gür, F.B. Prinz, J. Phys. Chem. Lett. 4 (2013) 1156.
[39] D. Marrocchelli, P.A. Madden, S.T. Norberg, S. Hull, Chem. Mater. 23 (2011) 1365.
[40] J.P. Goff, W. Hayes, S. Hull, M.T. Hutchings, K.N. Clausen, Phys. Rev. B 59 (1999) 14202.
[41] M. De Ridder, R. Van Welzenis, H. Brongersma, U. Kreissig, Solid State Ion. 158 (2003) 67.
[42] T. Ryll, H. Galinski, L. Schlagenhauf, P. Elser, J.L. Rupp, A. Bieberle-Hutter, L.J. Gauckler, Adv. Funct. Mater. 21 (2011) 565.
[43] J.S. Park, T.P. Holme, J.H. Shim, F.B. Prinz, MRS Commun. 2 (2012) 107.